Composites Science and Technology 70 (2010) 450–457

Contents lists available at ScienceDirect

Composites Science and Technology

journal homepage: www.elsevier.com/locate/compscitech

Static deformations of functionally graded polar-orthotropic cylinders with elliptical inner and circular outer surfaces

G.J. Nie [a,b], R.C. Batra [b,*]

[a] School of Aerospace Engineering and Applied Mechanics, Tongji University, Shanghai 200092, China

[b] Department of Engineering Science and Mechanics, M/C 0219, Virginia Polytechnic Institute and State University, Blacksburg, VA 24061, USA

ARTICLE INFO

Article history:
Received 7 August 2009
Received in revised form 9 November 2009
Accepted 22 November 2009
Available online 26 November 2009

Keywords:
A. Functionally graded materials
B. Hollow circular cylinder with elliptic inner surface
C. Analytical solution
D. Stress analysis
E. Material tailoring

ABSTRACT

Functionally graded materials (FGMs) enable one to tailor the spatial variation of material properties so as to fully use the material everywhere. For example, in a hollow circular cylinder one can vary, in the radial direction, the material moduli to make the hoop stress constant. Whereas the problem for a hollow cylinder with the inner and the outer surfaces circular has been studied, that of a cylinder with a circular outer surface and a non-circular inner surface or vice versa has not been investigated. We study here such a plane-strain problem when the cylinder material is polar-orthotropic, material properties vary exponentially in the radial direction, and deformations are independent of the axial coordinate. The problem is challenging since the cylinder thickness varies with the angular position of a point, and the cylinder material is inhomogeneous. Equilibrium equations are solved by expanding the radial and the circumferential displacements in Fourier series in the angular coordinate. The method of Frobenius series is used to solve ordinary differential equations for coefficients of the Fourier series, and boundary conditions are satisfied in the sense of Fourier series. A parametric study has been conducted that delineates effects on stresses of the eccentricity of the ellipse, the material property gradation index and loads applied on boundaries of the cylinder. The analytical solutions presented here will serve as benchmarks for comparing solutions derived by numerical methods.

1. Introduction

Functionally graded materials (FGMs) are composites composed of two or more phases with the composition and the morphology gradually changing in or more directions resulting in continuous variation of the material elasticities with the spatial position. An advantage of FGMs is that one can tailor the spatial variation of material properties to fully use the material everywhere. For example, the radial variation of the material moduli of a FG cylinder can be found to attain a constant hoop stress in the cylinder. However, the spatial variation of elastic properties complicates the analysis and the design of FG structures. From mathematics point of view, one needs to solve partial differential equations with variable coefficients; accordingly the solution of pertinent boundary-value problems (BVPs) is more challenging. There is extensive literature on the mechanical behavior of FG structures (for example, see [1–6]).

We review below the pertinent literature on the investigation of stresses and displacements in a FG hollow circular cylinder composed of isotropic and linear elastic materials. Horgan and Chan [7] analyzed two-dimensional plane stress/strain deformations by assuming Young's modulus $E(r)$ to be a power law function of the radius r and constant Poisson's ratio υ. Oral and Anlas [8] discussed the stress distribution in an inhomogeneous anisotropic cylinder; Pan and Roy [9] solved a plane-strain problem for a FG cylinder by dividing it into several homogeneous cylinders. Tutuncu [10] gave the power series solution for stresses and displacements in FG cylinders, and Theotokoglou and Stampouloglou [11] studied axisymmetric problems for radially inhomogeneous circular cylinders. The effect of varying υ on deformation fields in FG cylinders has been investigated by Mohammadi and Dryden [12]. Li and Peng [13] have analyzed axisymmetric deformations of FG hollow cylinders and disks with arbitrarily varying material properties. Zimmerman and Lutz [14], Jabbari et al. [15,16], Liew et al. [17], Shao et al. [18,19], and Hosseini et al. [20] have analyzed thermoelastic problems for FG cylinders or cylindrical panels. Ootao et al. [21,22], Afsar and Sekine [23], and Goupee and Vel [24] have optimized material compositions for inhomogeneous hollow circular cylinders.

We note that deformations of a hollow cylinder with a circular outer surface and a non-circular inner surface or vice versa have not been investigated. Design considerations may dictate a non-circular cross-section of a cylinder; for example, several naval and flight vessels are non-circular, and oil tanks have elliptical outer surfaces. Dynamic and buckling characteristics of elliptic cylinders are quite different from those of circular cylinders; for example see [25,26]. Here we study plane-strain static

* Corresponding author.
E-mail address: rbatra@vt.edu (R.C. Batra).

0266-3538/$ - see front matter © 2009 Elsevier Ltd. All rights reserved.
doi:10.1016/j.compscitech.2009.11.018

deformations of a cylinder with elliptical inner and circular outer surfaces composed of a material that is polar-orthotropic and its moduli vary exponentially in the radial direction. The problem is challenging since the cylinder thickness varies with the angular position of a point and material properties vary in the radial direction. The analytical solution of the problem is obtained by employing the Fourier and the Frobenius series, and effects of geometric and material parameters on the solution of the problem are delineated.

2. Problem formulation

Consider an infinitely long cylinder shown in Fig. 1 of uniform cross-section with elliptical inner surface concentric with the outer circular surface. The lengths of the major and the minor semi-axes of the elliptical inner surface are a_{in} and b_{in}, respectively, and the radius of outer circular surface is r_{ou}. Because the cylinder geometry, the material properties, and the applied loads are independent of the axial coordinate of a point, the state of deformation in the cylinder is assumed to be that of plane-strain. We take the origin of the cylindrical coordinate axes at the center of ellipse, and denote coordinates of a point in a cross-section by (r, θ).

For a plane-strain problem, equations of equilibrium in cylindrical coordinates (r, θ), in the absence of body forces, are

$$\frac{\partial \sigma_{rr}}{\partial r} + \frac{1}{r}\frac{\partial \sigma_{r\theta}}{\partial \theta} + \frac{\sigma_{rr} - \sigma_{\theta\theta}}{r} = 0, \quad \frac{\partial \sigma_{\theta r}}{\partial r} + \frac{1}{r}\frac{\partial \sigma_{\theta\theta}}{\partial \theta} + \frac{2}{r}\sigma_{\theta r} = 0,$$
$$\tilde{r}(\theta) < r < r_{ou}, \tag{1}$$

where σ_{rr}, $\sigma_{r\theta} = \sigma_{\theta r}$ and $\sigma_{\theta\theta}$ are stress components. The function $\tilde{r}(\theta)$ is given by

$$\tilde{r}(\theta) = b_{in}/\sqrt{1 - e^2\cos^2\theta}, \tag{2}$$

where $e = \sqrt{1 - b_{in}^2/a_{in}^2}$ is the eccentricity of the elliptical inner surface.

The radial and the circumferential displacements, u_r and u_θ, are related to the strains ε_{rr}, $\varepsilon_{\theta\theta}$ and $\varepsilon_{r\theta}$ through the following relations:

$$\varepsilon_{rr} = \frac{\partial u_r}{\partial r}, \quad \varepsilon_{\theta\theta} = \frac{u_r}{r} + \frac{1}{r}\frac{\partial u_\theta}{\partial \theta}, \quad \varepsilon_{r\theta} = \frac{1}{r}\frac{\partial u_r}{\partial \theta} + \frac{\partial u_\theta}{\partial r} - \frac{u_\theta}{r}. \tag{3}$$

We assume that the cylinder is made of a polar-orthotropic linear elastic material with material elasticities varying in the radial direction. The constitutive relations are

$$\sigma_{rr} = c_{11}(r)\varepsilon_{rr} + c_{12}(r)\varepsilon_{\theta\theta}, \quad \sigma_{\theta\theta} = c_{12}(r)\varepsilon_{rr} + c_{22}(r)\varepsilon_{\theta\theta}, \quad \sigma_{r\theta} = c_{66}(r)\varepsilon_{r\theta}. \tag{4}$$

The elastic moduli, $c_{11}(r)$, $c_{22}(r)$, $c_{12}(r)$, $c_{66}(r)$, are assumed to be given by

$$c_{ij}(r) = c_{ij}^0 e^{\lambda\left(\frac{r}{r_{ou}}\right)} \quad (ij = 11, 22, 12, 66), \tag{5}$$

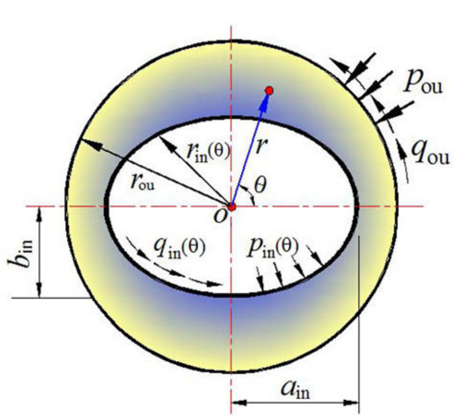

Fig. 1. Schematic sketch of the problem studied.

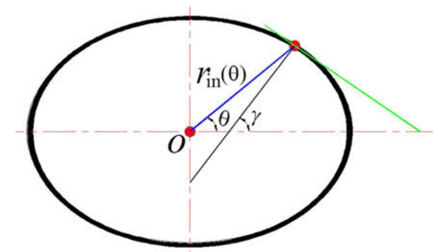

Fig. 2. Angles γ and θ for a point on the elliptical inner surface.

where λ is a constant. Thus the radial variation of the four elastic moduli is given by the same function.

Boundary conditions applied to the outer surface of the cylinder are

$$\text{either } \sigma_{rr}(r_{ou}, \theta) = -p_{ou}(\theta), \text{ or } u_r(r_{ou}, \theta) = \bar{u}_r^{ou}(\theta), \quad \text{and} \tag{6a, b}$$

$$\text{either } \sigma_{r\theta}(r_{ou}, \theta) = q_{ou}(\theta) \text{ or } u_\theta(r_{ou}, \theta) = \bar{u}_\theta^{ou}(\theta). \tag{6c, d}$$

Here $p_{ou}(\theta)$ and $q_{ou}(\theta)$ are the normal and the tangential tractions, respectively, assigned on the outer surface of the cylinder, and $\bar{u}_r^{ou}(\theta)$ and $\bar{u}_\theta^{ou}(\theta)$ are, respectively, the prescribed radial and the circumferential displacements there. Functions $p_{ou}(\theta)$, $q_{ou}(\theta)$, $\bar{u}_r^{ou}(\theta)$ and $\bar{u}_\theta^{ou}(\theta)$ are such that they can be expressed as Fourier series in θ. On the elliptical inner surface of the cylinder, displacements are prescribed as

$$u_r(\tilde{r}(\theta), \theta) = \bar{u}_r^{in}(\theta), \quad u_\theta(\tilde{r}(\theta), \theta) = \bar{u}_\theta^{in}(\theta), \tag{7a, b}$$

where $\bar{u}_r^{in}(\theta)$ and $\bar{u}_\theta^{in}(\theta)$ are known functions of θ. Traction boundary conditions on the elliptical inner surface of the cylinder are

$$\sigma_{rr}(\tilde{r}(\theta), \theta)\cos(\gamma - \theta) + \sigma_{r\theta}(\tilde{r}(\theta), \theta)\sin(\gamma - \theta)$$
$$= -p_{in}(\theta)\cos(\gamma - \theta) + q_{in}(\theta)\sin(\gamma - \theta), \tag{8a}$$

$$\sigma_{r\theta}(\tilde{r}(\theta), \theta)\cos(\gamma - \theta) + \sigma_{\theta\theta}(\tilde{r}(\theta), \theta)\sin(\gamma - \theta)$$
$$= -p_{in}(\theta)\sin(\gamma - \theta) + q_{in}(\theta)\cos(\gamma - \theta), \tag{8b}$$

where $p_{in}(\theta)$ and $q_{in}(\theta)$ are the normal and the tangential tractions applied on the inner surface, and the angle γ between the normal of the inner surface and the horizontal axis, as shown in Fig. 2, is given by [27]

$$\tan\gamma = \frac{a_{in}}{b_{in}}\tan\theta. \tag{9}$$

For an arbitrary shape of the inner surface of the cylinder it is difficult to exactly satisfy traction boundary conditions (8). Therefore, we approximately satisfy them by dividing the surface into several small straight segments, and equate the central angle θ of an arbitrary segment *i* to the average of central angles of two ends of the segment. We expand prescribed functions on the boundary in terms of Fourier series in θ, multiply both sides of Eqs. (6)–(8) by $\cos(m\theta)$ and $\sin(m\theta)$, integrate numerically by using the Gauss quadrature rule from 0 to 2π, and solve the resulting system of algebraic equations for coefficients of Fourier series.

When only surface tractions are prescribed on the inner and the outer surfaces, then the assigned surface tractions must have null resultant force and moment in order for the problem to have a solution.

3. Problem solutions

We assume that the displacement fields can be expressed as [9,15]

$$u_r(r,\theta)=\sum_{m=0}^{\infty}[u^c_{rm}(r)\varphi^c_m+u^s_{rm}(r)\varphi^s_m],$$
$$u_\theta(r,\theta)=\sum_{m=0}^{\infty}[u^c_{\theta m}(r)\varphi^c_m+u^s_{\theta m}(r)\varphi^s_m], \tag{10a, b}$$

where integer m equals the circumferential wave number, $\varphi^c_m=\cos(m\theta)$, $\varphi^s_m=\sin(m\theta)$, and superscripts c and s signify quantities associated with the cosine and the sine terms. For non-axisymmetric problems, we take $u^s_{r0}=u^s_{\theta 0}=0$ since they do not contribute to u_r and u_θ respectively.

For $m = 0$, substitution for displacements u_r and u_θ from Eqs. (10a,b) into Eq. (3), and then for strains into Eq. (4), and stresses into Eq. (1) gives the following 2nd order ordinary differential equation for u^c_{r0} and $u^c_{\theta 0}$:

$$c^0_{11}\frac{d^2u^c_{r0}}{dr^2}+c^0_{11}\left(\frac{1}{r}+\frac{\lambda}{r_{ou}}\right)\frac{du^c_{r0}}{dr}+\left(\frac{\lambda c^0_{12}}{r_{ou}r}-\frac{c^0_{22}}{r^2}\right)u^c_{r0}=0, \tag{11a}$$

$$\frac{d^2u^c_{\theta 0}}{dr^2}+\left(\frac{1}{r}+\frac{\lambda}{r_{ou}}\right)\frac{du^c_{\theta 0}}{dr}-\left(\frac{\lambda}{r_{ou}r}+\frac{1}{r^2}\right)u^c_{\theta 0}=0. \tag{11b}$$

Thus for $\lambda = 0$ (i.e., a homogeneous cylinder), solutions of Eqs. (11a,b) are

$$u^c_{r0}=C_{10}r^h+C_{20}r^{-h},\quad u^c_{\theta 0}=C_{01}r+C_{02}r^{-1} \tag{12a, b}$$

and for $\lambda\neq 0$, Eqs. (11a,b) have the solutions

$$u^c_{r0}=\exp(-h_r+h\ln r)(C_{30}U(-h_1,1+2h,h_r)+C_{40}L^{2h}_{h_1}(h_r)), \tag{13a}$$

$$u^c_{\theta 0}=C_{03}r+C_{04}r(\exp(-h_r)(\lambda r_{ou}/r-r^2_{ou}/r^2)+\lambda^2\mathrm{Ei}(-h_r)), \tag{13b}$$

where $h=\sqrt{c^0_{22}/c^0_{11}}$, $h_r=\lambda r/r_{ou}$, $h_1=h^2-h-1$; constants of integration C_{10}, C_{20}, C_{30}, C_{40}, C_{01}, C_{02}, C_{03} and C_{04} are determined by boundary conditions, $L^{2h}_{h_1}(z)$ is the generalized Laguerre polynomial, $U(g_1,g_2,z)=1/\Gamma(g_1)\int_0^\infty e^{-zt}t^{g_1-1}(1+t)^{g_2-g_1-1}dt$ is the confluent hypergeometric function, and $\mathrm{Ei}(z)$ is the exponential integral function. We note that only those values of the gradation index λ are admissible for which the hypergeometric function has a finite value.

For $m\geqslant 1$, following the same procedure as above we obtain the following 2nd order differential equations for u^c_{rm}, u^s_{rm} and $u^c_{\theta m}, u^s_{\theta m}$:

$$\sum_{m=1}^{\infty}\left[f_{1m}(r)\varphi^c_m+f_{2m}(r)\varphi^s_m\right]=0,\quad \sum_{m=1}^{\infty}\left[f_{3m}(r)\varphi^c_m+f_{4m}(r)\varphi^s_m\right]=0. \tag{14a, b}$$

Here

$$\begin{aligned}
f_{1m}(r)&=c^0_{11}\frac{d^2u^c_{rm}}{dr^2}+c^0_{11}g_1(r)\frac{du^c_{rm}}{dr}+g_2(r)u^c_{rm}+g_3(r)\frac{du^s_{\theta m}}{dr}+g_4(r)u^s_{\theta m},\\
f_{2m}(r)&=c^0_{11}\frac{d^2u^s_{rm}}{dr^2}+c^0_{11}g_1(r)\frac{du^s_{rm}}{dr}+g_2(r)u^s_{rm}-g_3(r)\frac{du^c_{\theta m}}{dr}-g_4(r)u^c_{\theta m},\\
f_{3m}(r)&=c^0_{66}\frac{d^2u^c_{\theta m}}{dr^2}+c^0_{66}g_1(r)\frac{du^c_{\theta m}}{dr}-g_5(r)u^c_{\theta m}+g_3(r)\frac{du^s_{rm}}{dr}+g_6(r)u^s_{rm},\\
f_{4m}(r)&=c^0_{66}\frac{d^2u^s_{\theta m}}{dr^2}+c^0_{66}g_1(r)\frac{du^s_{\theta m}}{dr}-g_5(r)u^s_{\theta m}\\
&\quad -g_3(r)\frac{du^c_{rm}}{dr}-g_6(r)u^c_{rm}.
\end{aligned} \tag{15a, b, c, d}$$

and

$$\begin{aligned}
g_1(r)&=\frac{1}{r}+\frac{\lambda}{r_{ou}},\quad g_2(r)=\frac{\lambda c^0_{12}}{r_{ou}r}-\frac{c^0_{22}+m^2c^0_{66}}{r^2},\\
g_3(r)&=\frac{m(c^0_{12}+c^0_{66})}{r},\quad g_4(r)=\frac{\lambda mc^0_{12}}{r_{ou}r}-\frac{m(c^0_{22}+c^0_{66})}{r^2},\\
g_5(r)&=\frac{\lambda c^0_{66}}{r_{ou}r}+\frac{c^0_{66}+m^2c^0_{22}}{r^2},\quad g_6(r)=\frac{\lambda mc^0_{66}}{r_{ou}r}+\frac{m(c^0_{22}+c^0_{66})}{r^2}.
\end{aligned}$$

Equating to zero coefficients of $\cos(m\theta)$ and $\sin(m\theta)$ on both sides of Eq. (14) gives

$$f_{1m}(r)=0,\quad f_{2m}(r)=0,\quad f_{3m}(r)=0,\quad f_{4m}(r)=0. \tag{16a, b, c, d}$$

We note that u^c_{rm} and $u^s_{\theta m}$ are obtained by simultaneously solving Eqs. (16a,d), and u^s_{rm} and $u^c_{\theta m}$ by simultaneously solving Eqs. (16b,c). These equations are solved by the method of Frobenius series. First, we non-dimensionalize displacements $u^c_{rm}, u^s_{\theta m}, u^s_{rm}$, $u^c_{\theta m}$ and the radial coordinate r by r_{ou}, and elastic constants c_{11}, c_{22}, c_{12}, c_{66} by c_{11}. Henceforth we use non-dimensional variables and denote them by the same symbols as before.

We assume that the Fourier components of displacements have the following power series expansion.

$$u^c_{rm}(r)=\sum_{k=0}^{\infty}a_kr^{k+t_1},\quad u^s_{\theta m}(r)=\sum_{k=0}^{\infty}b_kr^{k+t_1},$$
$$u^s_{rm}(r)=\sum_{k=0}^{\infty}c_kr^{k+t_2},\quad u^c_{\theta m}(r)=\sum_{k=0}^{\infty}d_kr^{k+t_2}, \tag{17a, b, c, d}$$

where constants a_k, b_k, c_k, d_k ($k = 0, 1, 2, \ldots$) are given by the recurrence formulae, $a_0, b_0, c_0, d_0\neq 0$, and exponents t_1 and t_2 are determined as a part of the solution of the problem.

Substituting for u^c_{rm} and $u^s_{\theta m}$ from Eq. (17a,b) into Eq. (16a,d) and equating to zero coefficients of the same power of r, we get the following recurrence formulae for a_k and b_k:

$$f^0_{11}a_0+f^0_{12}b_0=0, f^0_{21}a_0+f^0_{22}b_0=0, \tag{18a, b}$$

$$F_1a_k+F_2b_k=F_3a_{k-1}+F_4b_{k-1},$$
$$F_5a_k+F_6b_k=F_7a_{k-1}+F_8b_{k-1},\quad k=1,2,3\ldots, \tag{18c, d}$$

where

$$\begin{aligned}
f^0_{11}&=-c^0_{22}-c^0_{66}m^2+c^0_{11}t_1^2,\\
f^0_{12}&=-m(c^0_{22}-c^0_{12}t_1+c^0_{66}-c^0_{66}t_1),\\
f^0_{21}&=-m(c^0_{22}+c^0_{12}t_1+c^0_{66}+c^0_{66}t_1),\\
f^0_{22}&=-c^0_{22}m^2-c^0_{66}+c^0_{66}t_1^2,\\
F_1&=-c^0_{22}-c^0_{66}m^2+c^0_{11}(k+t_1)^2,\\
F_2&=m(-c^0_{22}+c^0_{66}(-1+k+t_1)+c^0_{12}(k+t_1)),\\
F_3&=\lambda(c^0_{12}+c^0_{11}(-1+k+t_1))/r_{ou},\\
F_4&=\lambda mc^0_{12}/r_{ou},\\
F_5&=-m(c^0_{22}+c^0_{12}(k+t_1)+c^0_{66}(1+k+t_1)),\\
F_6&=-c^0_{22}m^2+c^0_{66}(k^2+2kt_1+t_1^2-1),\\
F_7&=-\lambda mc^0_{66}/r_{ou},\\
F_8&=c^0_{66}\lambda(-2+k+t_1)/r_{ou}.
\end{aligned}$$

Assuming that $f_{12} = 0$, we find b_0 from Eq. (18a) as

$$b_0=-f^0_{11}a_0/f^0_{12}. \tag{19}$$

Equating to zero the determinant of the coefficient matrix of a_0 and b_0 in Eq. (18a,b), we get the following equation for the exponent t_1:

$$c^0_{11}c^0_{66}t_1^4+ct_1^2+c^0_{22}c^0_{66}(m-1)^2(m+1)^2=0, \tag{20}$$

where $c=-(c^0_{11}+c^0_{22})c^0_{66}+(c^0_{12}(2c^0_{66}+c^0_{12})-c^0_{11}c^0_{22})m^2$. Eq. (20) can be analytically solved for t_1 and we omit the lengthy expression.

Solutions of Eq. (16a,d) are

$$u^c_{rm}(r)=\sum_{j=1}^{4}\sum_{k=0}^{\infty}C_ja^j_kr^{k+t^j_1},\quad u^s_{\theta m}(r)=\sum_{j=1}^{4}\sum_{k=0}^{\infty}C_jb^j_kr^{k+t^j_1}, \tag{21a, b}$$

where constants C_j ($j = 1, 2, 3, 4$) are determined from boundary conditions in Eqs. (6)–(8).

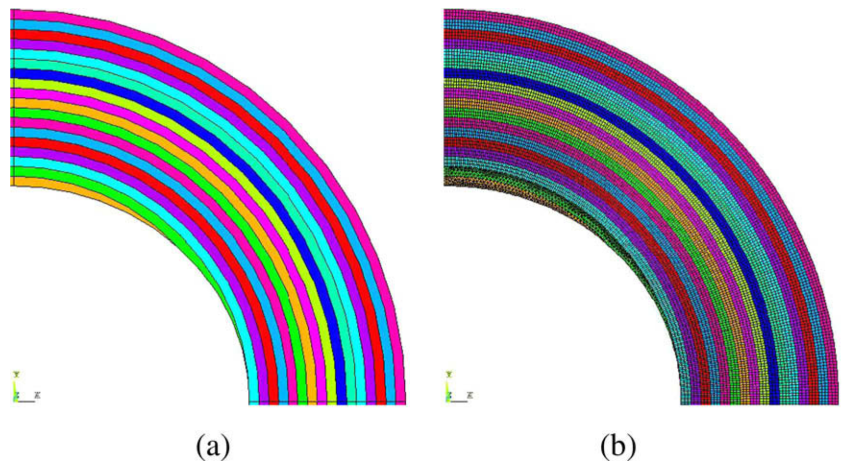

Fig. 3. A quarter of the cylinder divided into (a) several layers, and (b) the FE mesh for solving the problem by the FEM.

Following the same procedure as above, we get solutions of Eq. (16b,c) as

$$u_{rm}^{s}(r)=\sum_{j=1}^{4}\sum_{k=0}^{\infty}D_j c_k^j r^{k+t_2^j},\quad u_{\theta m}^{c}(r)=\sum_{j=1}^{4}\sum_{k=0}^{\infty}D_j d_k^j r^{k+t_2^j}, \tag{21c, d}$$

where constants D_j (j = 1, 2, 3, 4) are determined from the boundary conditions.

Substituting for u_{r0}^{c} and $u_{\theta 0}^{c}$ from Eq. (12a,b) or (13a,b) and for $u_{rm}^{c}, u_{\theta m}^{s}, u_{rm}^{s}$ and $u_{\theta m}^{c}$ ($m > 0$) from Eq. (21a–d) into Eq. (10a,b), we get analytical solutions for displacements of the FG cylinder. Note that Eq. (11) can also be solved for u_{r0}^{c} *and* $u_{\theta 0}^{c}$ by the Frobenius series method following the same procedure as above, and the problem may no solution for some values of the graded index λ. because special functions in Eq. (13) may not be well defined. Knowing displacements, stresses can be computed.

4. Example problems

4.1. Convergence of the series solution

Example 1: Consider a FG cylinder with lengths of the major and the minor semi-axes of the elliptical inner surface as a_{in} = 0.6 m and b_{in} = 0.55 m, respectively, the radius of the circular outer surface r_{ou} = 1.0 m, and vales of material parameters as

$$c_{11}(r)=1.0\exp(6r/r_{ou})\ \text{GPa},\quad c_{22}(r)=c_{11}(r),$$
$$c_{12}(r)=0.343c_{11}(r),\quad c_{66}(r)=0.328c_{11}(r).$$

For the pressure, 1.0 MPa, applied on the elliptical inner surface and the circular outer surface fixed, results are compared with those obtained from the commercial finite element software, ANSYS, realizing that the finite element method (FEM) provides an approximate solution of a BVP whose accuracy can be improved upon by increasing the number of elements into which the problem domain is divided. For analyzing the problem with ANSYS, a quarter of the cylinder is divided into two parts – one a circular cylinder of inner radius 0.6 m and outer radius 1.0 m, and the other of thickness 0.05 m at $\theta = \pi/2$ and 0 at θ = 0. The first part of uniform thickness is divided into 16 equal parts in the radial direction with uniform material properties equal to those at the center assigned to these thin cylinders. The FE mesh for each thin cylinder has three (800) uniform elements in the radial (circumferential) direction. The second portion of the cylinder of thickness 0.05 m at $\theta = \pi/2$ and 0 at θ = 0 is divided into two homogeneous thin layers composed of 4808 triangular elements, as shown in Fig. 3. The total number of nodes and elements in the FE mesh equal 41,485 and 43,208, respectively. Values of elastic moduli in each layer are constants and equal those obtained from Eq. (5) at the midpoint of the layer. Boundary conditions resulting from the symmetry of the problem (i.e., null tangential tractions and zero normal displacements) are applied to nodes on the horizontal and the vertical planes. For results presented in Fig. 4 below, '*a*' and '*p*' represent, respectively, solutions obtained with the FEM and the present approach, and '*m*' denotes the circumferential wave number of the external pressure. It is clear that results from the two approaches agree well with each other. We note that the present (FEM)

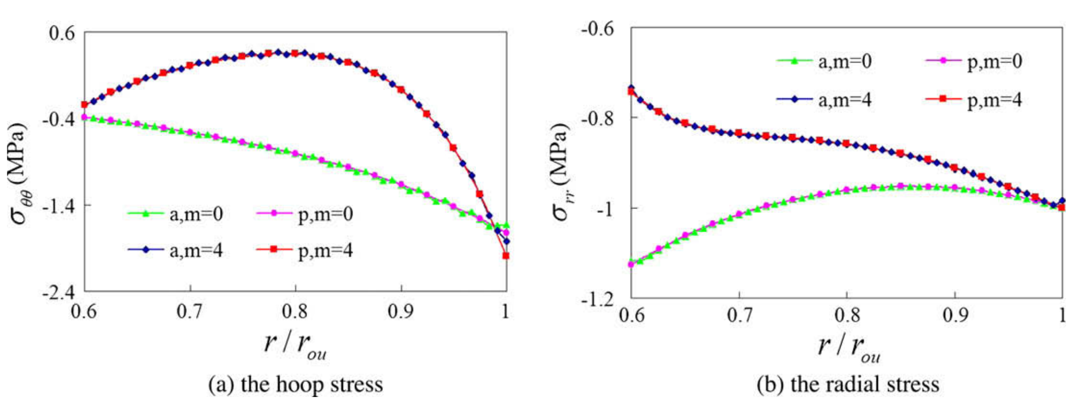

Fig. 4. Variation in the radial direction of (a) the hoop stress, and (b) the radial stress.

Table 1
Effect of the number of Gauss points and the number of terms in the Fourier and the Frobenius series on the radial stress at the point (0.625 m, 0).

Gaussian points	Number of terms in the Fourier series–number of terms in the Frobenius series					
	6–30	6–40	8–30	8–40	12–30	12–40
64	−0.96584	−0.96584	−0.96577	−0.96577	−0.96576	−0.96576
128	−0.96585	−0.96585	−0.96576	−0.96576	−0.96569	−0.96569

The radial stress at the point (0.625 m, 0) from ANSYS is −0.96086 MPa.

approach involves 480 (82,970) unknowns; thus the proposed method for this problem is computationally more efficient than the FEM.

For 64 and 128 Gauss points used to numerically evaluate integrals, and different number of terms retained in the Fourier and the Frobenius series, we have listed in Table 1 values of the radial stress at the point (0.625 m, 0). It is clear that the value of the radial stress hardly changes when either 6 (30) or 8 (40) terms in the Fourier (Frobenius) series and either 64 or 128 Gauss points are used to numerically evaluate integrals. Furthermore, the radial stress obtained from the present method differs from that computed with the FEM by less than 0.5%.

Note that the number of terms in the Frobenius and the Fourier series needed to obtain a converged solution varies with the eccentricity of the elliptical inner surface of the cylinder and the gradation of material properties. Therefore, in the following examples, the number of terms in these series is increased till stresses at a point have converged to within 0.1% of their values.

4.2. Parametric studies

We investigate through numerical examples the influence of (i) the gradation of material properties, (ii) non-uniform external pressures, and (iii) the eccentricity of the elliptical inner surface on displacements and stresses induced in FG cylinders. For results presented below, unless otherwise noted, the elliptical inner surface is fixed, the pressure applied on the circular outer surface equals either 1.0 MPa or $1.0 \times \cos(4\theta)$ MPa, number of terms in the Fourier series for displacements = 8, number of terms in the Frobenius series for the coefficient of each term is the Fourier series = 30, number of Gauss points used to numerically evaluate integrals = 128.

4.2.1. The effect of the gradation of material properties

Example2: For $\lambda = -6$, 0 and 6, and uniform pressure on the outer surface = 1.0 MPa, through-the-thickness distributions of the radial and the hoop stresses along the major and the minor semi-axes of the inner ellipse are exhibited in Fig. 5. Note that the cylinder thickness is minimum for the radial line $\theta = 0$, maximum along the radial line $\theta = \pi/2$, and results for $\lambda = 0$ are for a homogeneous cylinder. Whereas $\lambda = -6$ makes the hoop stress essentially uniform on the two radial lines in the cylinder, the maximum magnitude of the radial stress is greater than that for the homogeneous cylinder. Stresses plotted in Fig. 5a–d illustrate that the magnitude of the hoop stress on the radial line $\theta = \pi/2$ increases significantly at points in the vicinity of the outer surface

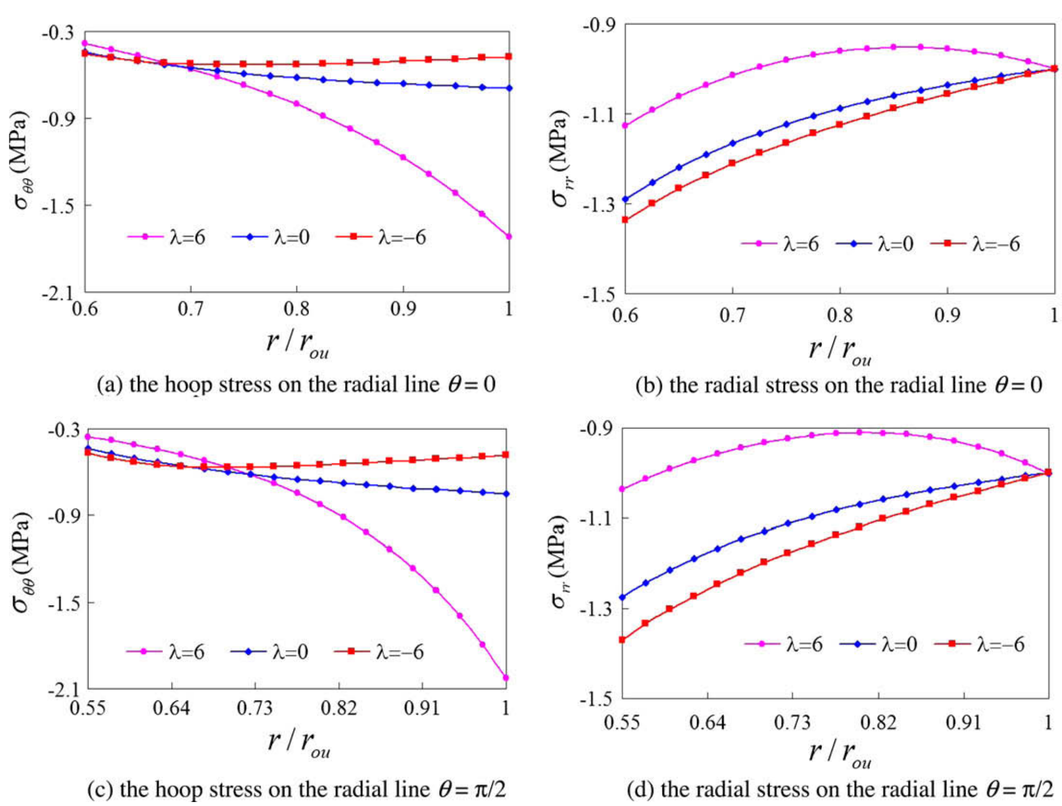

Fig. 5. For three values of the gradation index λ of material properties, through-the-thickness distributions of (a) the hoop stress on the line $\theta = 0$, (b) the radial stress on the line $\theta = 0$, (c) the hoop stress on the line $\theta = \pi/2$, and (d) the radial stress on the line $\theta = \pi/2$.

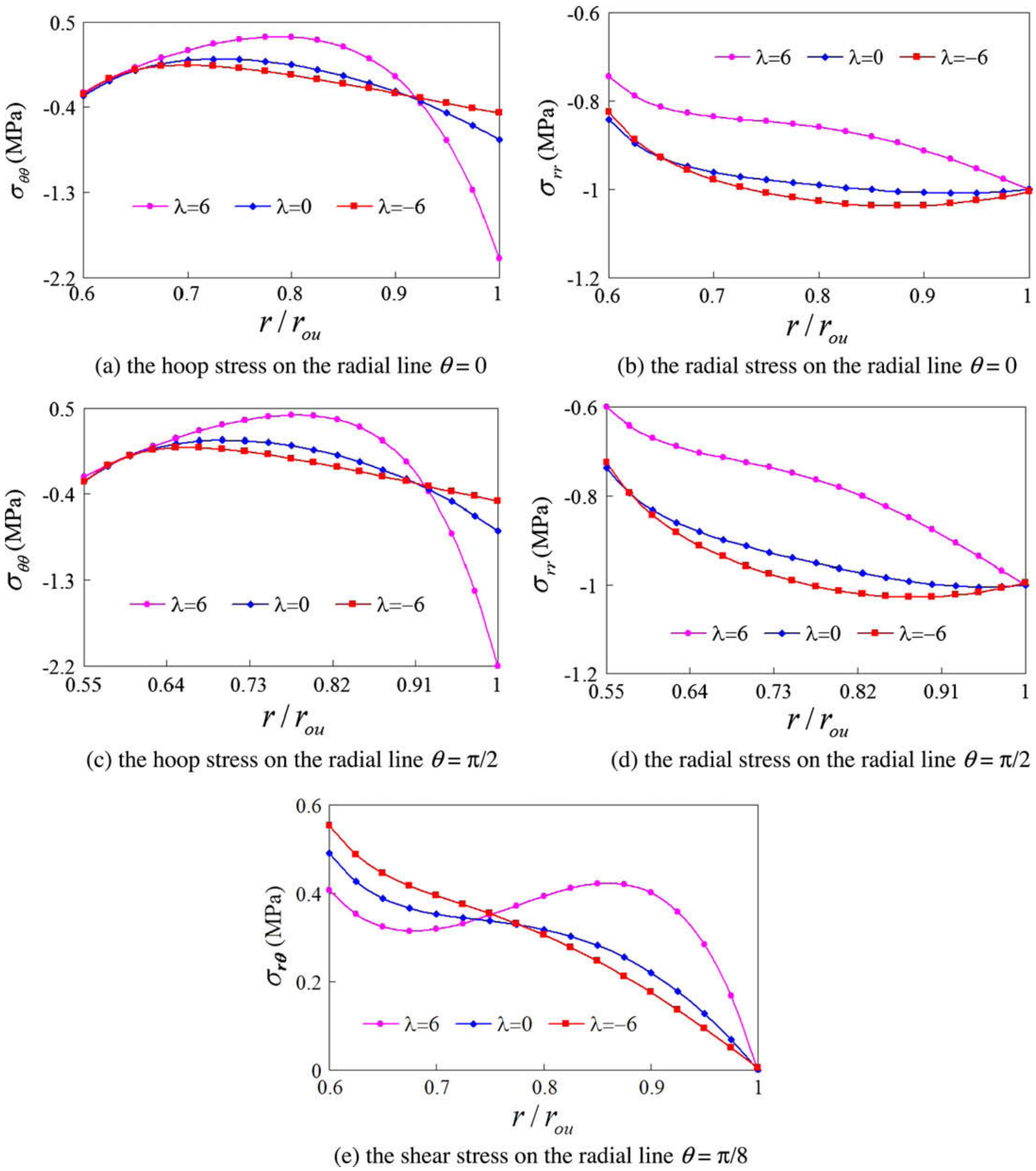

Fig. 6. For three values of the graded index of the material properties, through-the-thickness distributions of (a) the hoop stress on the radial line $\theta = 0$, (b) the radial stress on the radial line $\theta = 0$, (c) the hoop stress on the radial line $\theta = \pi/2$, (d) the radial stress on the radial line $\theta = \pi/2$, and (e) the shear stress on the radial line $\theta = \pi/8$.

for $\lambda = 6$, and the magnitude of the radial stress on the line $\theta = \pi/2$ increases noticeably at points near the inner surface for $\lambda = -6$. The difference in stresses on the radial lines $\theta = 0$ and $\theta = \pi/2$ reveals the influence of the inner elliptical surface (or of the variation of the thickness) of the cylinder. The shear stress at a point in the cylinder is considerably less than the magnitude there of the normal stresses, and is thus not plotted here.

4.2.2. The effect of non-axisymmetric external pressures

Example 3: For the BVP of example 2 except that the pressure on the outer surface is given by $1.0 \times \cos(4\theta)$ MPa, through-the-thickness stress distributions are displayed in Fig. 6. The value of a quantity at a point (r, θ) is obtained by multiplying the value of the quantity at the point $(r, 0)$ by $\cos(4\theta)$.

Through-the-thickness distributions of stresses on the two radial lines differ noticeably from those shown in Fig. 5, and signify the effect of non-axisymmetric pressure applied on the outer surface of the cylinder. Whereas for a uniform pressure the hoop stress is compressive everywhere (see Fig. 5a and c), for a non-uniform pressure it can be tensile at an interior point of the cylinder (see Fig. 6a and c). Due to the eccentricity of the inner elliptical surface, on the radial line $\theta = \pi/2$, the hoop stress at points near the outer surface is greater than that at the corresponding points on the line $\theta = 0$ for $\lambda = 6$. Whereas the shear stress in example 2 for the uniform pressure case is very small, that for the non-uniform pressure loading is comparable in magnitude to the normal stresses at points on the inner clamped surface.

4.2.3. The effect of the eccentricity of elliptical inner surface

Example 4: For the cylinder considered in example 1, we now vary length of the minor axis to alter the eccentricity of the inner elliptic surface. For $b_{in} = 0.5, 0.55, 0.6$ m, and the cylinder outer surface subjected to a uniform pressure 1.0 MPa, Fig. 7 exhibits through-the-thickness distributions of the radial and the hoop stresses when $\lambda = -6$ and 6.

The through-the-thickness distributions of two stresses depend continuously upon the eccentricity of the inner elliptic surface. For $\lambda = -6$, the radial stress at a point on the line $\theta = \pi/2$ is

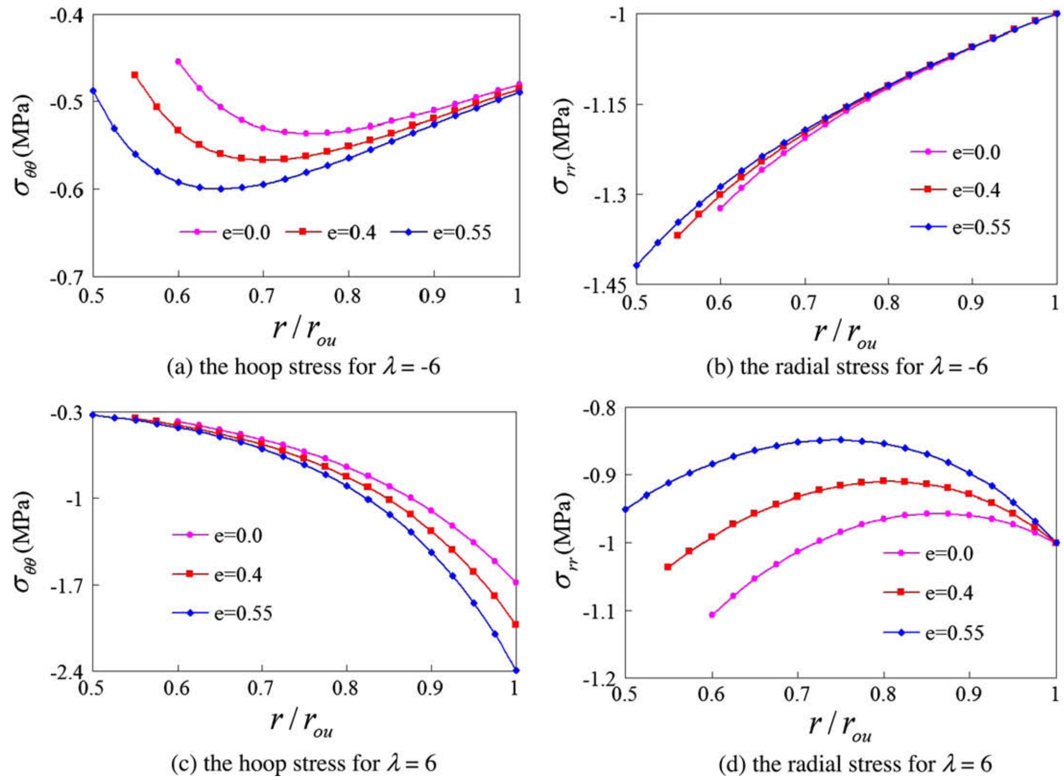

Fig. 7. For three values of the eccentricity of the inner elliptic surface, through-the-thickness distributions on the radial line $\theta = \pi/2$ of (a) the hoop stress for $\lambda = -6$, (b) the radial stress for $\lambda = -6$, (c) the hoop stress for $\lambda = 6$, and (d) the radial stress for $\lambda = 6$.

not affected much by the eccentricity on the inner surface but the maximum magnitude of the hoop stress increases with an increase in e. However, for $\lambda = 6$, with an increase in e, the maximum value of the hoop stress increases but that of the radial stress decreases.

5. Conclusions

We have studied analytically static plane-strain deformations of functionally graded polar-orthotropic cylinders with elliptic inner and circular outer surfaces by employing the Fourier and the Frobenius series and assuming that the four relevant elastic moduli have the same exponential variation in the radial direction. The radial and the circumferential displacements are expanded in Fourier series in the angular coordinate and the ordinary differential equations for coefficients of the Fourier series are solved by using the Frobenius series method. Boundary conditions are satisfied in the sense of Fourier series. The stresses obtained with the present method are found to agree very well with those computed with the finite element method using commercial software with the cylinder thickness divided into several contiguous perfectly bonded homogeneous cylinders. It is found that the distributions of the hoop and the radial stresses along different radial lines are noticeably affected by the gradation of material properties, the wave number of the pressure applied on the outer surface, and the eccentricity of the inner surface. An inappropriate value of the gradation index may adversely affect stresses at a point in the sense that it may significantly increase rather than decrease their magnitudes. Also, the sign of the hoop stress at a point depends strongly upon the value of the gradation index.

The analytical solutions presented here can serve as benchmark solutions for comparing results computed with other numerical algorithms.

Acknowledgements

This work was supported by the office of Naval Research Grant N00014-06-1-0567 to Virginia Polytechnic Institute and State University with Dr Y.D.S. Rajapakse as the program manager. Views expressed in the paper are those of authors, and neither of the funding agency nor of authors' institutions.

References

[1] Chen CS, Hsu CY, Tzou GJ. Vibration and stability of functionally graded plates based on a higher-order deformation theory. J Reinf Plast Compos 2009;28(10):1215–34.
[2] Nejad M Zamani, Rahimi GH. Deformations and stresses in rotating FGM pressurized thick hollow cylinder under thermal load. Sci Res Essay 2009;4(3):131–40.
[3] Jin X, Wu LZ, Sun YG, et al. Microstructure and mechanical properties of ZrO_2/NiCr functionally graded materials. Mater Sci Eng A 2009;509:63–8.
[4] Alibeigloo A. Static analysis of a functionally graded cylindrical shell with piezoelectric layers as sensor and actuator. Smart Mater Struct 2009;18:1–12.
[5] Nemat Alla M, Ahmed KIE, Hassab Allah I. Elastic–plastic analysis of two-dimensional functionally graded materials under thermal loading. Int J Solids Struct 2009;46:2774–86.
[6] Khabbaz RS, Manshadi BD, Abedian A. Nonlinear analysis of FGM plates under pressure loads using the higher-order shear deformation theories. Compos Struct 2009;89:333–44.
[7] Horgan CO, Chan AM. Pressurized hollow cylinder or disk problem for functionally graded isotropic linear elastic materials. J Elast 1999;55(1):43–59.
[8] Oral A, Anlas G. Effects of radially varying moduli on stress distribution of nonhomogeneous anisotropic cylindrical bodies. Int J Solids Struct 2005;42(20):5568–88.
[9] Pan E, Roy AK. A simple plane-strain solution for functionally graded multilayered isotropic cylinders. Struct Eng Mech 2006;24(6):727–40.
[10] Tutuncu. Stresses in thick-walled FGM cylinders with exponentially-varying properties. Eng Struct 2007;29:2032–5.
[11] Theotokoglou EE, Stampouloglou IH. The radially nonhomogeneous elastic axisymmentric problem. Int J Solids Struct 2008;45:6535–52.
[12] Mohammadi Mohsen, Dryden JR. Influence of the spatial variation of Poisson's ratio upon the elastic field in nonhomogeneous axisymmetric bodies. Int J Solids Struct 2009;46:788–95.

[13] Li Xian Fang, Peng Xu Long. A pressurized functionally graded hollow cylinder with arbitrarily varying material properties. J Elast 2009;96:81–95.
[14] Zimmerman Robert W, Lutz Melanie P. Thermal stresses and thermal expansion in a uniformly heated functionally graded cylinder. J Therm Stress 1999;22:177–88.
[15] Jabbari M, Sohrabpour S, Eslami MR. General solution for mechanical and thermal stresses in a functionally graded hollow cylinder due to nonaxisymmetric steady-state loads. J Appl Mech 2003;70:111–8.
[16] Jabbari M, Vaghari AR, Bahtui A, et al. Exact solution for asymmetric transient thermal and mechanical stresses in FGM hollow cylinders with heat source. Struct Eng Mech 2008;29(5):551–65.
[17] Liew KM, Kitipornchai S, Zhang XZ, et al. Analysis of the thermal stress behavior of functionally graded hollow circular cylinders. Int J Solids Struct 2003;40:2355–80.
[18] Shao ZS, Wang TJ. Three-dimensional solutions for the stress fields in functionally graded cylindrical panel with finite length and subjected to thermal/mechanical loads. Int J Solids Struct 2006;43:3856–74.
[19] Shao ZS, Ang KK, Reddy JN, et al. Nonaxisymmetric thermomechanical analysis of functionally graded hollow cylinders. J Therm Stress 2008;31(6):515–36.
[20] Hosseini SM, Akhlaghi M, Shakeri M. Heat conduction and heat wave propagation in functionally graded thick hollow cylinder base on coupled thermoelasticity without energy dissipation. Heat Mass Trans 2008;44(12):1477–84.
[21] Ootao Y, Kawamura R, Tanigawa Y, Imamura R. Optimization of material composition of nonhomogeneous hollow circular cylinder for thermal stress relaxation making use of neural network. J Therm Stress 1999;22(1):1–22.
[22] Ootao Y, Tanigawa Y, Nakamura T. Optimization of material composition of FGM hollow circular cylinder under thermal loading: a neural network approach. Composites Part B 1999;30:415–22.
[23] Afsar AM, Sekine H. Optimum material distributions for prescribed apparent fracture toughness in thick-walled FGM circular pipes. Int J Pressure Vessels Piping 2001;78(7):471–84.
[24] Goupee AJ, Vel SS. Multi-objective optimization of functionally graded materials with temperature-dependent material properties. Mater Des 2007;28(6):1861–79.
[25] Soldatos KP. Mechanics of cylindrical shells with non-circular cross-section: a survey. Appl Mech Rev 1999;52:237–74.
[26] Patel BP, Gupta SS, Loknath MS, Kadu CP. Free vibration analysis of functionally graded elliptical cylindrical shells using higher-order theory. Compos Struct 2005;69:259–70.
[27] Nagaya K, Hai Y. Free vibration of composite membranes with arbitrary shape. J Sound Vib 1985;100(1):123–34.